

Model predictive control for an SAPF interfaced by a wind energy conversion system based on permanent magnet synchronous generator

Abdelkader Lakhdari*, Fateh Krim* and Abdelhalim Borni**

* *Laboratoire d'Electronique de Puissance et Commande Industrielle (LEPCI), Université de Sétif 1, Algeria*

** *Unité de Recherche Appliquée en Energies Renouvelables, URAER, Centre de Développement des Energies Renouvelables CDER, 47133, Ghardaïa, Algeria*

* *Corresponding Author: lakhdari_abdelkader@hotmail.com*

ABSTRACT

This paper deals with the connection of a wind generation system to the grid through a shunt active power filter (SAPF), which is used mostly to improve the power quality, compensate the reactive power, and reduce the distortion appeared on the grid current waveforms produced by the connected non-linear loads. Another task assigned to the SAPF is to inject the active power extracted from the wind system to the power grid, ensuring a load power sharing. The SAPF is a three-phase two-level inverter controlled by a predictive current control and is fed by a wind system through a DC-link capacitor; a PI regulator is synthesized to fix the DC-bus voltage at a constant value and compensate the system losses. The wind system composed of a wind turbine coupled to a gearless permanent magnetic synchronous generator (PMSG) aims to convert the mechanical energy available on the shaft to an electrical energy. Because of the fluctuating and unpredictable nature of the wind and its speed variation, an uncontrolled three-phase diode rectifier connected to a DC/DC boost converter is used to control and feed the electric power extracted from the wind system to the DC-link. MATLAB Simulink simulations show the effectiveness of the used control system to improve the grid current waveforms, to compensate the reactive power, and to ensure a continuous injection of the wind power to the point of common coupling (PCC) to share the load power with the grid.

Keywords : DC/DC converter; harmonics; PMSG; shunt active power filter; wind system.

INTRODUCTION

Faced with the depletion of fossil energy resources and environmental issues caused by the emission of greenhouse gases in the exploitation of these resources, many so-called renewable energy resources have been emerged such as photovoltaic, wind, biomass, etc. Wind energy is among the best ones shared by all the inhabitants of the earth; it comes from the conversion of kinetic energy of the wind into mechanical energy by the favor of a turbine. This mechanical energy is exploited to rotate the rotor of an electric generator to produce an electric energy.

For high power scales, a doubly fed induction generator is usually then used. But for low power scales, the Permanent Magnet Synchronous Generator (PMSG) is the most used because of the advantages it has: absence of the excitation circuit, gearless generator (no gearbox block), high efficiency, and low maintenance.

On the other side, the great and quick development in the manufacture of the electronic components made the modern power systems able to contain the combination of linear and nonlinear loads. In recent years, the intensive use of power electronic elements (transistor, thyristor...etc) as switching devices of power converters (such as diode or thyristor rectifiers) is being increased vastly. As a result, harmonics are still being generated from the nonlinear loads that forced the power system operates at low power factor, low efficiency, distorted current and voltage waveforms, and increased losses in transmission and distribution lines (Yiauw & Khanniche, 2001).

To overcome these disturbances, active filtering has proven effective as an alternative to solutions based on passive filters; the shunt active filter is based on the injection of harmonic currents equal, and in opposite phase to those generated by the nonlinear load in a coupling point to force the grid currents to be sinusoidal (Chellali, 2005, Khadem et al. 2014).

The active filter is a voltage two-level inverter aiming to inject with a proper control harmonic currents needed to feed the non-linear load in order to save the sinusoidal waveforms of the grid currents.

The conventional methods such as the instantaneous p-q theory (Khadkikar et al., 2009), synchronous reference frame (SRF) theory (Ochoa-Gimnez et al., 2015 ; Sundaram & Venugopal, 2016), and direct power control (DPC) (Djazia et al., 2015) are very used because their simple control implementation. But the low dynamic performance and their bandwidth limitation decrease the compensation quality. Furthermore, the absence of a phase locked loop (PLL) makes these methods unfit variable frequency systems (Chilipi et al., 2018). In this paper, an intelligent current predictive control based on a discrete model of SAPF is proposed; the high accuracy and the simple concept and implementation of this method make it an attractive alternative to the classical control methods. The principle of this method is based on the selection among the all eight possible voltage vectors of the SAPF the optimal voltage vector that minimizes a predefined cost function. The grid reference currents are extracted from the DC-bus control loop dedicated to maintaining the DC-bus voltage fixe and close to its reference value using a PI controller.

The rest of the paper is presented as follows: Section 2 presents a literature review. Section 3 presents the configuration of the system under study. Section 4 describes the wind system modeling details. Section 5 explains the current predictive control proposed to control the SAPF. Afterwards, simulation results are presented in Section 6. Finally, the paper is concluded in Section 7.

LITERATURE REVIEW

Many studies treat the harmonic pollution problem solutions based on active filters. Rahmani et al. (2012) proposed a Lyapunov function control for a hybrid parallel filter to mitigate the harmonics applied for balanced operation. Chen et al. (2012) developed an aircraft active filter used to improve the voltage quality in close-loop way. Mikkili & Panda (2012) developed two control techniques based on PI (Proportional/Integral) regulator and fuzzy logic controller. Komurcugil (2015) proposed a double-band hysteresis current control for a single phase inverter based SAPF in the goal to achieve a lower average frequency and lower switching losses compared to the classic single band hysteresis control.

After that the researchers became interested in the association of the active filters and renewable energy resources (single source or hybrid systems) in order to assign another task to the active filter besides of the reduction of harmonic pollution, which is the injection of the active power produced by the renewable sources to the grid. Boukezata et al. (2014) proposed a photovoltaic system associated with a shunt active filter controlled by a hysteresis direct current control. Vaikundaselvan & Ranithottungal (2014) presented a wind energy system associated with an active filter controlled by a synchronous reference frame theory technique and space vector pulse width modulation. Ouchen et al. (2016a) developed a real time implementation of a fuzzy-predictive direct power control for an SAPF connecting photovoltaic system to the grid, where a fuzzy logic based maximum power point tracking control to track at any moment the optimal point of the photovoltaic generator is performed. Ouchen et al. (2016b) proposed an experimental validation of a sliding mode-predictive direct power control to interface a small scale photovoltaic system to the grid, where a fuzzy logic based maximum power point tracking control to track at any moment the optimal point of the photovoltaic generator is developed. Boukezata et al. (2016) proposed a multifunctional grid connected inverter interfaced by a PV system, where a new predictive technique is applied to control the SAPF based on the prediction of the generated filter current.

This paper proposes the connection of a wind generation system to the grid through a two-level inverter based SAPF and at the same time performs reactive power compensation and reduces the grid current harmonic distortions using the model predictive control. The last exploits the model of the whole system (SAPF + grid + load) to select among the all eight possible voltage vectors of the SAPF the optimal voltage vector that minimizes a predefined cost function. The selected cost function is based on the prediction of the grid currents instead of filter currents in order to eliminate the disturbances in the network. These disturbances come from the connected nonlinear load absorbing non-sinusoidal currents, the presence of reactive power, or imbalances introduced by constrained networks (Albuquerque et al., 2010; Ilango et al., 2012; Tummuru et al., 2014).

Figure 1 shows the principle scheme of an SAPF interfaced by a wind energy system:

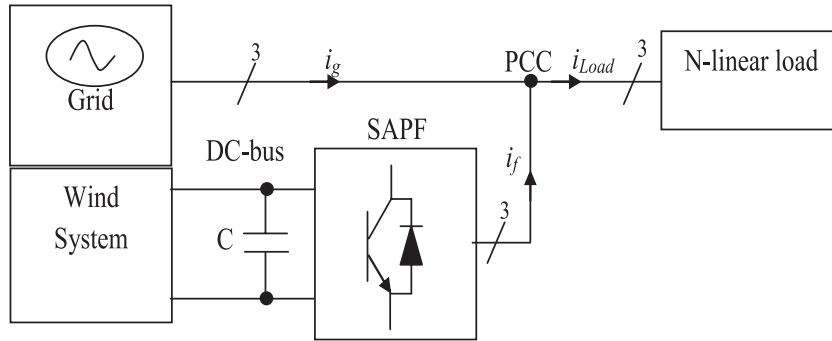


Figure 1. Principle scheme of an SAPF fed by a wind system.

SYSTEM CONFIGURATION

The studied system consists of an SAPF, which is a three-phase two-level inverter controlled by predictive current control and is fed by a wind system through a DC-bus capacitor. The power that reached the DC-link is fed to the PCC through the SAPF. At the PCC and in parallel with the grid and the filter, a nonlinear load (which is a three-phase diode rectifier coupled to a resistance in series with an inductor) is connected. A passive filter (inductive) is connected at the end of the SAPF to reduce the current harmonics.

The wind generation system consists of a three-blade wind turbine, which transforms the kinetic energy from the wind in mechanical torque applied on the shaft, the shaft drives directly (no gearbox block) the shaft of a PMSG, and a three-phase diode rectifier coupled to a DC/DC boost converter is responsible to transfer the power generated by the generator (AC side) to the DC-bus (DC side).

The generator side and the grid side are coupled by a DC-link, which used to keep the SAPF input voltage constant and close to its reference value to compensate the power losses. The system has two main functions: at full-windy days, the power generated by the wind system is fed to the load through the SAPF. If this power exceeds the load needs, the excess of power will be injected to the grid. At low-windy days (the injected wind power is less than the load requirements), the grid will share the load by giving the difference of power to meet the load power need. During no wind periods, the power required by the load is received from the grid while the SAPF only gives reactive power compensation and the needed harmonic currents.

Figure 2 shows the proposed system topology associated with the SAPF:

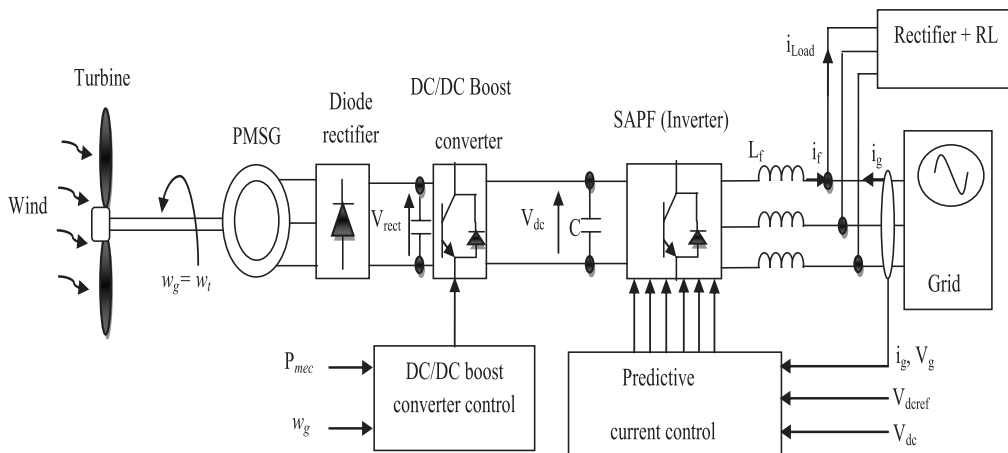


Figure 2. Scheme of the proposed wind system connected through an SAPF.

WIND ENERGY SYSTEM

The expression of power converted by the turbine into mechanical power from the wind is given by

$$P_{mec} = \frac{1}{2} \rho \pi R^2 C_p (\lambda, \beta) v^3 \quad (1)$$

where

P_{mec} : The mechanical power extracted from the wind.

ρ : The air density (kg / m^3).

R : The blade radius (m).

C_p : The power coefficient characterizing each turbine.

β : The pitch angle of the rotor blades in degrees.

v : The wind speed (m / s).

λ : The tip-speed ratio, and is given by:

$$\lambda = R \cdot \omega_t / v \quad (2)$$

where ω_t is the speed of the turbine shaft (rad / s).

The power coefficient C_p is a specific data characterizing each wind turbine, and it has a theoretical limit called ‘‘Betz limit’’. This limit is never being reached in practice (Laverdure, 2005). In this paper, the expression of the power coefficient in function of λ and the pitch angle β is given by the polynomial approximation (Figure 3) presented in (Dahbi, 2012)

$$C_p(\lambda, \beta) = (0.5 - 0.0167(\beta - 2)) \sin \left[\frac{\pi(\lambda + 0.1)}{18 - 0.3(\beta - 2)} \right] - 0.00184(\lambda - 3)(\beta - 2) \quad (3)$$

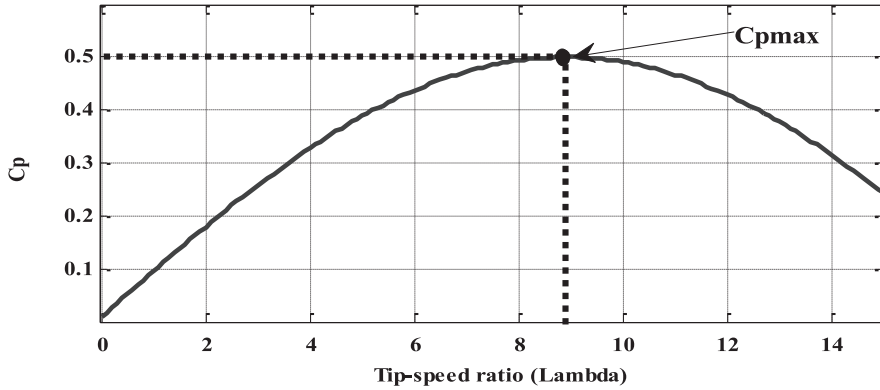


Figure 3. Power coefficient against tip-speed ratio.

The mechanical torque applied on the generator T_g is given by

$$T_g = P_g / \omega_g \quad (4)$$

where

P_g : is the mechanical power available on the generator shaft.

ω_g : is the speed of the generator shaft (rad / s)

By using a gearless generator, we can write

$$P_g = P_{mec} = \frac{1}{2} \rho \pi R^2 C_p (\lambda, \beta) v^3 \quad (5)$$

$$w_g = w_t \quad (6)$$

From (2), (4), (5), (6),

$$T_g = \frac{\rho \pi R^5 C_p(\lambda, \beta) w_g^2}{2 \lambda^3} \quad (7)$$

The mechanical equation of the system (turbine + generator) is presented in equation (8):

$$\begin{cases} J = J_t + J_g \\ J \cdot \frac{dw_g}{dt} = T_g - T_{em} - f_v \cdot w_g \end{cases} \quad (8)$$

where J_g and J_t are the moment of inertia of the generator and turbine, respectively; f_v indicates the generator viscous friction coefficient.

Permanent magnet synchronous generator

The dynamic model of the PMSG is presented in equation (9) where R_s is the stator resistant, L_d , L_q are the inductors in the dq frame, i_{ds} , i_{qs} are the stator currents in the dq frame, φ_f the radial flux of PMSG, and ω_e is the generator electric speed (Valenciaga & Puleston, 2008):

$$\begin{cases} \frac{di_{ds}}{dt} = -\frac{R_s}{L_d} i_{ds} + \frac{\omega_e \cdot L_q}{L_d} i_{qs} - \frac{V_{ds}}{L_d} \\ \frac{di_{qs}}{dt} = -\frac{R_s}{L_q} i_{qs} - \frac{\omega_e \cdot L_d}{L_q} i_{ds} + \frac{\omega_e (\varphi_f - V_{qs})}{L_q} \end{cases} \quad (9)$$

Equation (10) presents the generated electromagnetic torque:

$$T_{em} = \frac{3}{2} \cdot P \cdot \left((L_d - L_q) i_{ds} + \varphi_f \right) i_{qs} \quad (10)$$

$$L_d = L_q \quad (11)$$

$$T_{em} = \frac{3}{2} \cdot P \cdot \varphi_f \cdot i_{qs} \quad (12)$$

where P is the number of pair of poles.

Figure 4 shows the mechanical power against the rotor mechanical speed for variable wind speed:

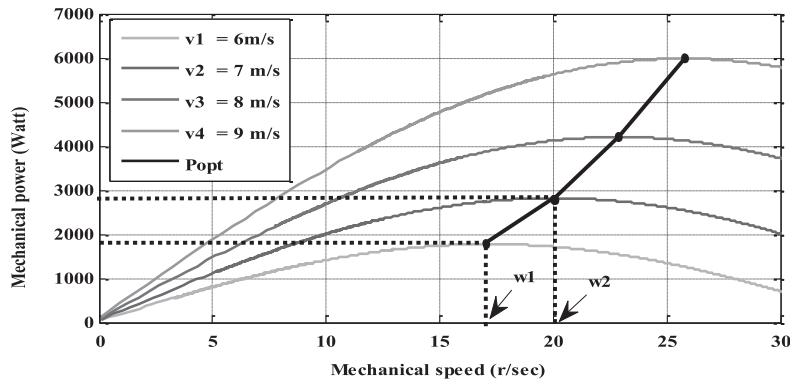


Figure 4. Mechanical power versus mechanical speed.

For a wind speed v_1 , the maximum output power is captured at w_1 . If the wind speed increases from v_1 to v_2 , the rotor speed is still fixed at w_1 . At this moment, the corresponding output power is less than the maximum power that can be extracted; hence the rotor speed should be increased from w_1 to w_2 (Esmaili, 2006). To extract the maximum available power at any wind speed; many maximum power point tracking (MPPT) algorithms based on mechanical speed control are proposed in the literature; the next section resumes the technique used to extract the corresponding maximum power for each wind speed.

Maximization of the extracted wind power

To control the speed of the PMSG, the optimum reference speed expressed by equation (13) was used:

$$w_{ref} = \frac{\lambda_{opt} \cdot v}{R} \tag{13}$$

The control topology of PMSG speed is illustrated in Figure 5:

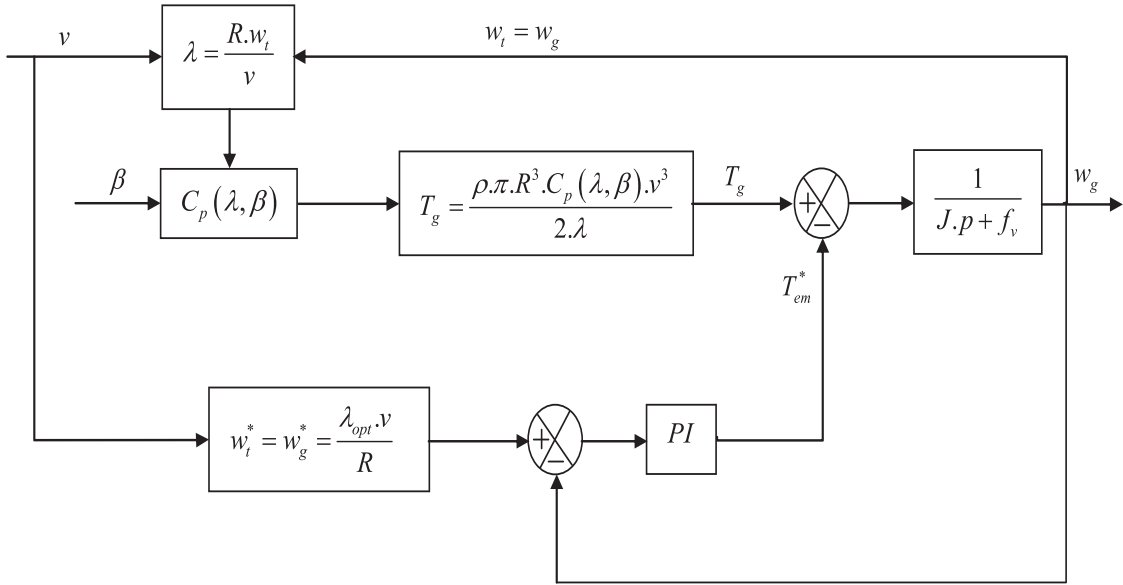


Figure 5. Block diagram of the power maximization with generator speed control.

Diode rectifier model

In this study, a three-phase diode rectifier is used. The diodes are assumed ideal and therefore their conduction corresponds to a short circuit and their blocking corresponds to an open circuit. Under these conditions, the two diodes, which lead to each sequence, correspond to the phase having the more positive voltage to the diode of the upper half-bridge and the phase having the more negative voltage to the diode of the lower half-bridge.

During each conduction sequence, the voltage V_{rect} at the rectifier output is

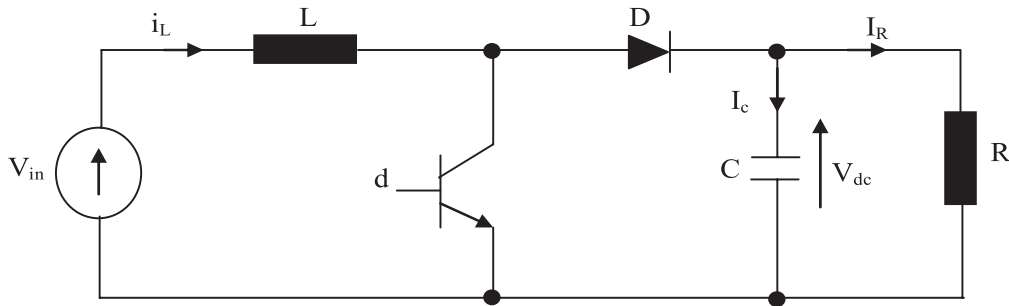
$$V_{rect} = \text{Max}(V_j) - \text{Min}(V_j); j = 1, 2, 3. \tag{14}$$

DC/DC boost converter

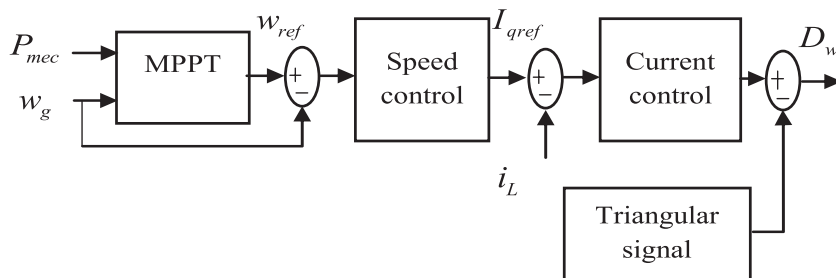
The basic circuit and control topology of the boost converter are depicted in Figure 6; the boost converter converts the rectified DC voltage into DC voltage in a desired value. Two conduction modes are operational. In mode 1, when the switch (transistor) is ON, the diode is in the OFF condition and the inductor stores energy. During this period, the capacitor supplies the output current. In mode 2, the switch is in the OFF condition; the capacitor stores energy and the energy stored in the inductor gets dissipated. The state equation that describes the behavior of the boost converter in the two modes is expressed in (15):

$$\begin{cases} \frac{di_L}{dt} = \frac{d-1}{L}V_{dc} + \frac{V_{in}}{L} \\ \frac{dV_{dc}}{dt} = \frac{1-d}{C}i_L - \frac{1}{RC}V_{dc} \end{cases} \quad (15)$$

The inductor current is controlled on the basis of the mechanical speed error; as shown in Figure 6 (b), the speed error is the difference between the reference speed (from the MPPT block) and the actual speed. This error will be the input of a speed controller which is a PI regulator giving the reference inductor current (I_{qref}). This reference current will be compared to the boost inductor current, and the resulting error will be the input of another PI controller gives the control signal of the DC-DC converter.



(a)



(b)

Figure 6. Basic Circuit and control topology of the DC/DC boost converter.

(a) Basic circuit (b) Inductor current control.

MODEL PREDICTIVE CONTROL (MPC)

The base of the MPC is the prediction of the behavior of controlled variables using the model of the system. This information will be exploited by the controller to apply the optimal voltage vector among the large eight possible filter voltage vectors that minimizes a predefined cost function chosen according to the system control needs. For each voltage vector, the predicted value of the next sampling time is calculated and then, the switching sequence corresponding to the voltage vector, which minimizes the cost function, will be selected and sent to the filter switches.

This MPC technique applied in this work is summarized in the following steps (Rodriguez and Cortés, 2012; Rodriguez et al., 2007; Boukezata et al., 2016):

- Define an appropriate cost function J .
- Build the converter model and its possible switching sequences (voltage vectors).
- Build the SAPF model (associated with a non-linear load and fed by the grid) to extract the prediction law.

In Boukezata et al. (2016), the cost function used is minimizing the error between the predicted and reference values of the filter currents as written in equation (16):

$$J = \left| i_{f\alpha}^*(k+1) - i_{f\alpha}^p(k+1) \right| + \left| i_{f\beta}^*(k+1) - i_{f\beta}^p(k+1) \right| \quad (16)$$

where $i_{f\alpha}^p(k+1)$, $i_{f\alpha}^*(k+1)$ and $i_{f\beta}^p(k+1)$, $i_{f\beta}^*(k+1)$ refer to the real and imaginary components of the predicted and reference filter currents in the $\alpha\beta$ stationary frame, respectively.

In this work, the selected cost function is minimizing the error between the reference and predict values of the grid currents, which have the expression

$$J = \left| i_{g\alpha}^*(k+1) - i_{g\alpha}^p(k+1) \right| + \left| i_{g\beta}^*(k+1) - i_{g\beta}^p(k+1) \right| \quad (17)$$

where $i_{g\alpha}^p(k+1)$, $i_{g\alpha}^*(k+1)$ and $i_{g\beta}^p(k+1)$, $i_{g\beta}^*(k+1)$ are the real and imaginary components of the predict and reference grid current in the $\alpha\beta$ stationary frame.

But the grid reference current $i_g^*(k+1)$ is unknown; it can be predicted using its present and previous values using the second order extrapolation given in equation (18):

$$i_g^*(k+1) = 3i_g^*(k) - 3i_g^*(k-1) + i_g^*(k-2) \quad (18)$$

For a small sampling time, the approximation $i_g^*(k+1) = i_g^*(k)$ can be used and no extrapolation is needed (Rodriguez et al.; 2007). The SAPF reference currents are obtained by subtracting the grid reference current from the load currents as given in equation (19):

$$i_f^*(k+1) = i_{Load}(k+1) - i_g^*(k+1) \quad (19)$$

The proposed predictive current control is described by:

1. The grid current $i_g(k)$ is sensed and transformed to $\alpha\beta$ stationary frame, and the grid reference current $i_g^*(k)$ is obtained from the DC-link voltage control loop.
2. The SAPF model is used to calculate predicted value of the grid current in the next sampling time $i_g^p(k+1)$ for each vector of the eight possible voltage vectors.
3. The selected cost function J minimizes the error between the generated reference grid current and the predicted grid current calculated by the prediction law in the next sampling time for the all eight possible voltage vectors.
4. The voltage vector that minimizes the grid current error is selected and the corresponding optimal switching state signals are sent to the filter switches.

SAPF model

The one phase equivalent circuit of the system composed of SAPF + grid + nonlinear load is depicted in Figure 7 (Chaoui et al., 2013; Boukezata et al., 2016):

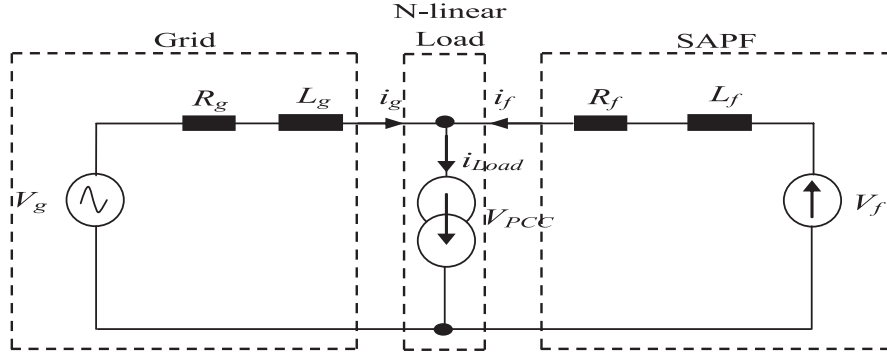


Figure 7. One phase equivalent circuit of an SAPF connected to a nonlinear load fed by the grid.

From Figure 7, the electrical equations can be written as

$$V_g - V_{PCC} = R_g * i_g + L_g \frac{di_g}{dt} \quad (20)$$

$$V_f - V_{PCC} = R_f * i_f + L_f \frac{di_f}{dt} \quad (21)$$

By subtracting equation (20) from equation (21) and neglecting the effects of the grid and filter resistances R_g and R_f respectively we find

$$V_g - V_f = L_g \frac{di_g}{dt} - L_f \frac{di_f}{dt} \quad (22)$$

But the load current is the sum of the fundamental current $i_{Load,f}$ and the harmonic current $i_{Load,h}$

$$i_{Load} = i_{Load,h} + i_{Load,f} \quad (23)$$

On the other hand,

$$i_{Load} = i_f + i_g \quad (24)$$

From equations (23) and (24), we obtain

$$i_{Load,h} + i_{Load,f} = i_f + i_g \quad (25)$$

Hence, we can write

$$i_{Load,h} - i_f = -(i_{Load,f} - i_g) \Rightarrow \Delta i_f = -\Delta i_g \quad (26)$$

For a small current variation, we can approximate $\Delta i \approx di$; equation (26) becomes

$$di_g = -di_f \quad (27)$$

By substituting equation (27) in equation (22), the final electrical equation can be given as

$$V_g - V_f = L_T \frac{di_g}{dt} / L_T = (L_g + L_f) \quad (28)$$

Discrete time model for prediction

This section describes the discretization of the grid current of the equation (28) for a sampling time T_s ; the discrete time model is essential to predict the future value of the grid current $i_g^p(k+1)$ using the present sampling time measured grid current $i_g(k)$, grid and filter voltages $V_g(k)$ and $V_f(k)$. Taking into account that the system is modeled as a first order model, the grid current derivative $\frac{di_g}{dt}$ can be substituted by a forward Euler approximation:

$$\frac{di_g}{dt} \approx \frac{i_g(k+1) - i_g(k)}{T_s} \tag{29}$$

By substituting approximation (29) in equation (28), the control law that gives the future values of the grid current for each vector voltage given by the SAPF is

$$i_g^p(k+1) = i_g^p(k) + \frac{T_s}{L_T} * (V_g(k) - V_f(k)) \tag{30}$$

The grid reference currents $i_g^*(k)$ are estimated by multiplying the output I_{gmax} , of a PI (proportional/integral) controller, which is used to compensate the losses in power and maintain the dc-bus voltage constant and close to its reference value V_{dcref} by a three-unit sinusoidal signal obtained from a phase locked loop (PLL) (Belhaouchet et al., 2007). This PLL is used to extract the phase of the grid voltages to synchronize the generated reference currents with the utility grid voltages.

Figure 8 shows the predictive current control block diagram used to control the SAPF:

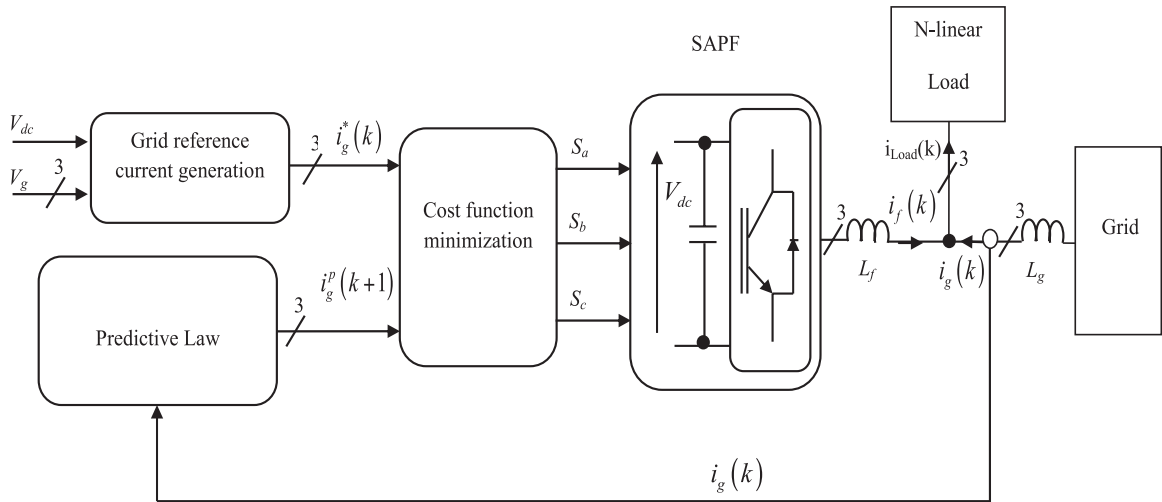


Figure 8. Principle scheme of the predict current control.

DC-bus control

In order to control the DC bus voltage and keep it close to its reference value required to feed the power circuit, a PI regulator will be used (Figure 9). First, the DC-bus voltage V_{dc} is measured by a voltage sensor then compared to a reference value (600 volts), the resulting error is corrected by the PI controller, the output of this control loop gives the reference peak current value of the I_{gmax} , and this current will be multiplied by a three unit sine ($\sin(\omega t)$, $\sin(\omega t + 2\pi/3)$, $\sin(\omega t + 4\pi/3)$), which are obtained from the PLL.

The controller will be synthesized by the following method:

The power absorbed by a capacitor is given by

$$P_f = \frac{d}{dt} \left(\frac{1}{2} \cdot C \cdot V_{dc}^2 \right) \quad (31)$$

After the Laplace transform,

$$V_{dc} = P_f \cdot \frac{1}{V_{dc}^* \cdot C \cdot p} \quad (32)$$

The PI controller transfer function is given by

$$K_p + \frac{K_i}{T_i} = \frac{1 + \tau \cdot p}{T_i \cdot p} \quad (33)$$

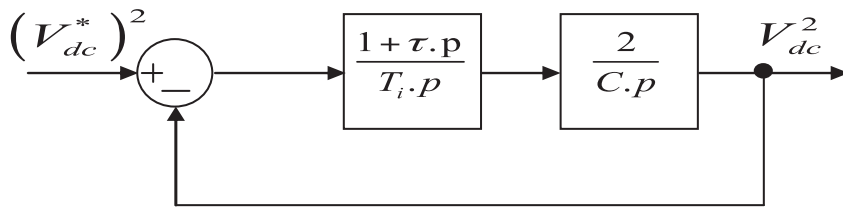


Figure 9. Functional control diagram of the DC bus voltage.

The transfer function in a closed loop $F(p)$ is given by

$$F(p) = \frac{w_0^2 \cdot (\tau \cdot p + 1)}{p^2 + 2\zeta w_0 \cdot p + w_0^2} / w_0 = \sqrt{\frac{2}{C \cdot T_i}}, \zeta = \frac{\tau}{\sqrt{2 \cdot C \cdot T_i}} \quad (34)$$

SIMULATION RESULTS

The simulations developed in this work are carried out using MATLAB/SIMULINK SimPowerSystem. The simulation shows the effectiveness of the active filter using a direct current control to compensate the reactive power and reject the current harmonics generated by the nonlinear load. Also, it shows the injection of the electric power extracted from wind system to the PCC.

Before the insertion of the SAPF and in direct connection between the grid and the non-linear load, the load consumes an active power reaches to (PL1 \approx 10 kW) as shown in Figure 10:

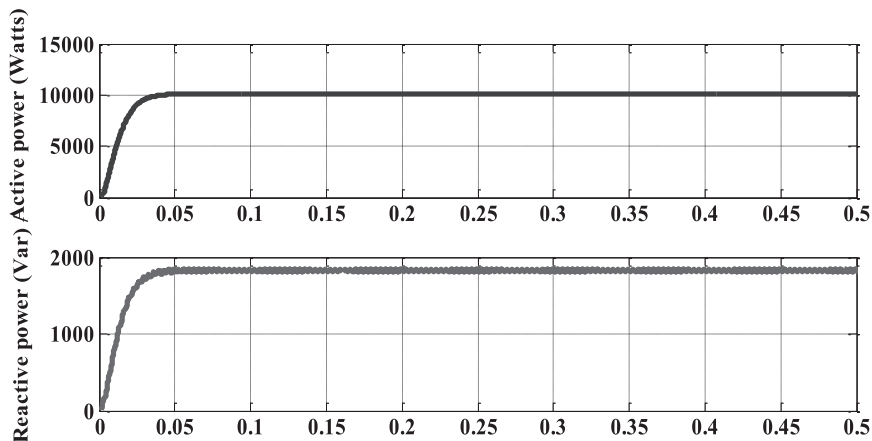


Figure 10. Active and reactive power consumed by the connected non-linear load before compensation.

Figure 11 shows the grid current waveforms and the corresponding spectral analysis; we can observe that the load consumes non-sinusoidal current with high total harmonic distortion in current ($THDi = 25.24\%$), which is greater than 5% (limit specified by IEEE standard 519–1992).

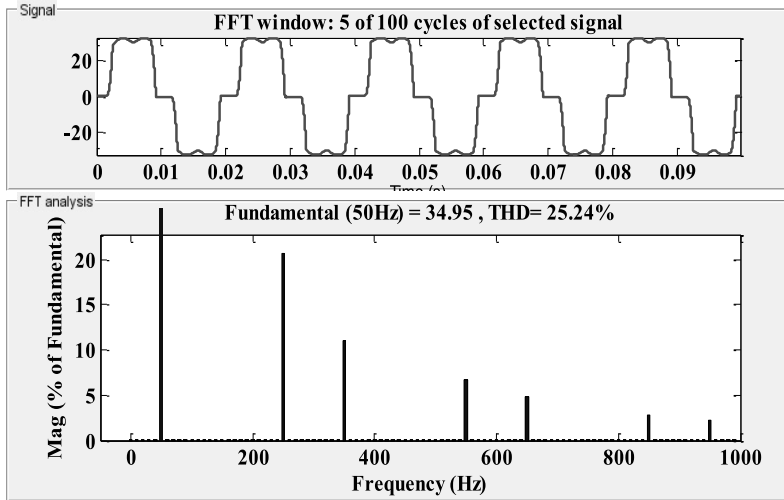


Figure 11. Waveforms and spectral analysis of the grid current (phase a).

After that, we re-run the system with the insertion of the active filter. The study is divided into two modes: the first mode shows the load power demand sharing between the grid and the renewable wind energy system, which occurred when the load power requirement is more than the power injected through the inverter. In this case, the grid gives the deficit of power to meet the load power requirements.

Figure 12 shows the wind profile (at $t = 0\text{sec}$, the wind speed $v = 9\text{m/s}$, then the speed decreases at $t = 0.4\text{sec}$ to $v = 7.5\text{m/s}$) and the corresponding maximum extracted power injected by the SAPF at each wind speed:

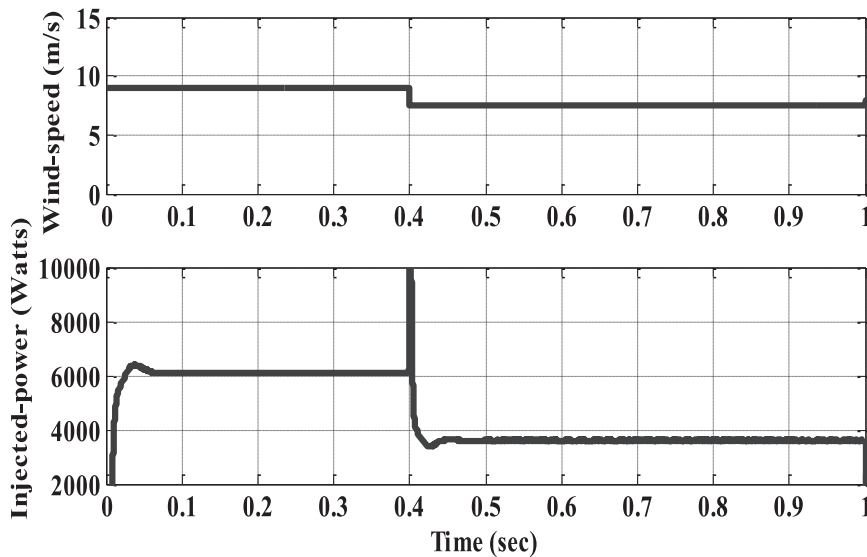


Figure 12. Wind speed profile and the corresponding maximum extracted power injected through the filter.

Figure 13 shows the effectiveness of the technique used to control the inductor current i_L of the boost converter. It is clear that current i_L follows its reference I_{qref} carefully and the variations in power and current generated by the wind system (Figure 12 and Figure 13) is consistent with the applied wind profile.

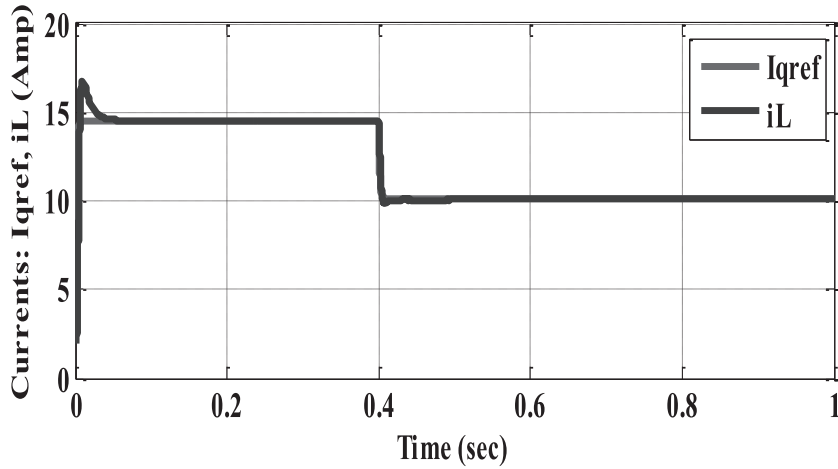


Figure 13. The boost inductor current and its reference.

Figures 14 and 15 show the load active power sharing; it can be observed from these Figures that the grid and the inverter work in conjunction and try to meet the load demand. Firstly, the power injected by the filter is greater than that injected by grid; when the power injected by the filter is decreased (wind speed decreases from $v = 9\text{m/s}$ to $v = 7.5\text{m/s}$), the grid will instantaneously increase its produced power to compensate the deficit of power.

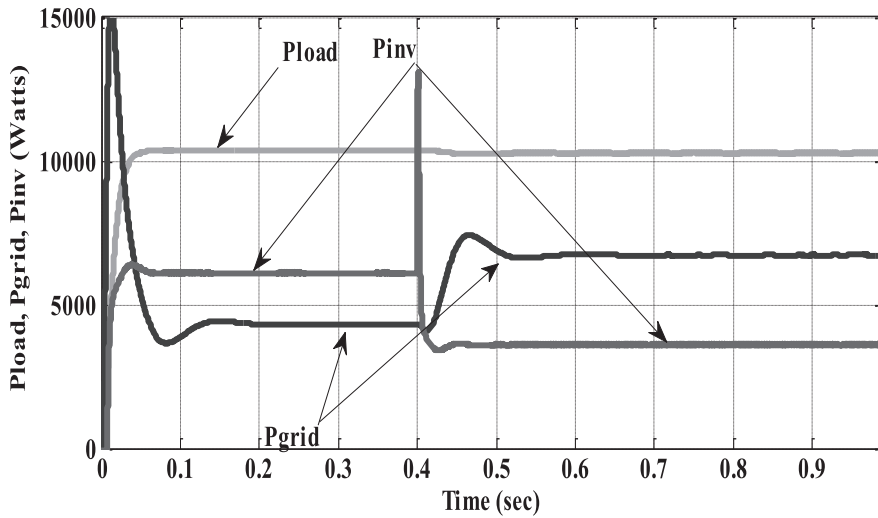


Figure 14. The load, grid, and filter powers.

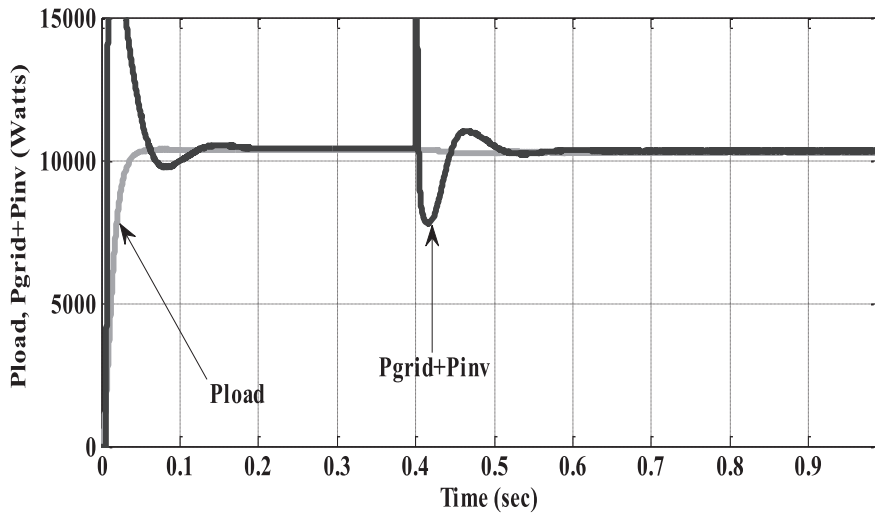


Figure 15. Load power sharing between the grid and the wind power injected by the filter.

Figure 16 shows the effectiveness of the SAPF to compensate the reactive power consumed by the connected nonlinear load; the compensation of the reactive is effective and therefore the reactive power of the network is zero, which means that this is the active filter that provides the reactive power to the load.

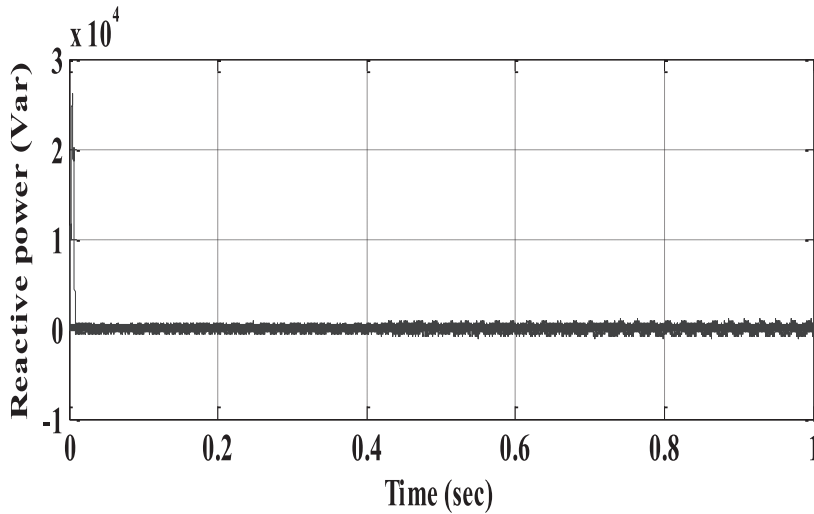


Figure 16. The grid reactive power.

Figure 17 proves that the PI controller succeeds to maintain the DC-bus voltage constant and close to its chosen reference value (600 volts) with a very small transition time ($\Delta t \approx 0.07$ sec):

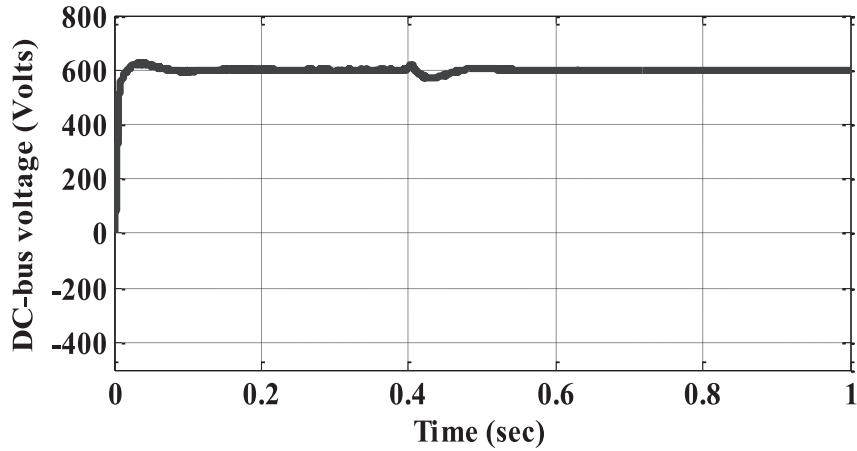


Figure 17. DC-bus voltage curve.

Figures 18 and 19 show the waveforms and the spectral analysis of the grid currents; these figures demonstrate the effectiveness of the proposed predictive current control to improve the waveforms of the grid currents. It can be seen from the value of the $THDi = 1.09\%$ that the MPC applied to the two-level inverter based SAPF provides a good prediction of the reference grid current and compensates clearly the grid reactive power (see Figure 16). The synchronization between the grid voltage and current (both are in phase) explains that the grid plays the role of a source to supply the deficit of power (positive power) needed to meet the load power demand.

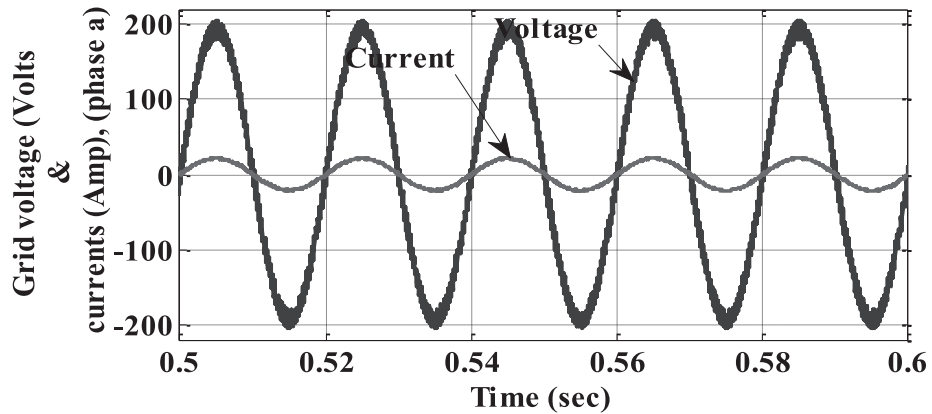


Figure 18. Grid current and voltage waveforms (phase a) after compensation.

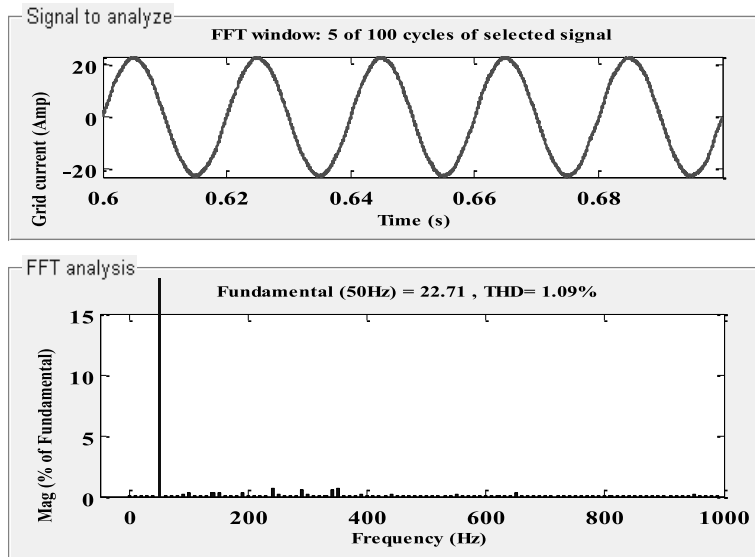


Figure 19. Waveforms and spectral analysis of the grid current after compensation.

Figure 20 shows the compensating current produced by our active filter to correct the imbalance in the system. It can be seen that the MPC succeeds to force the SAPF to generate the appropriate compensating current to improve the grid current waveforms.

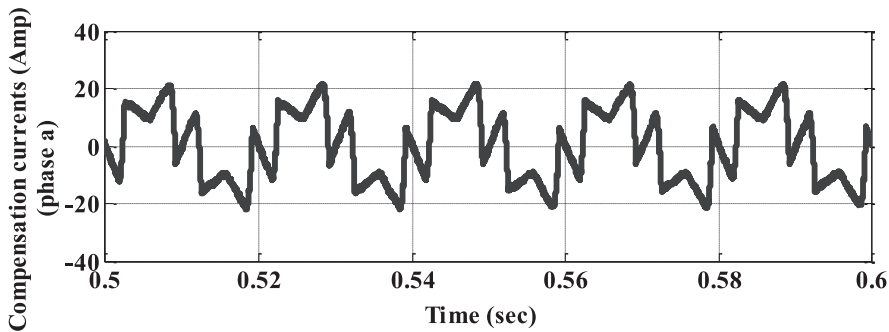


Figure 20. Compensation current injected by the filter (phase a).

The second mode occurred when the load power demand is less than the power injected by the filter. At $t = 1$ sec and for a wind speed $v = 8$ m/s, we introduce a load variation; the new connected load consumes an active power ($PL2 \approx 2.5$ kW). Figures 21 and 22 show the active power injected by the filter, the grid active power, and the load demand as well as the grid current and voltage waveforms after the load variation.

From Figures 21 and 22, it is seen that the active power injected through the filter is greater than that consumed by the load. The excess amount of power is transferred to the grid (with negative sign in Figure 21). As the voltage is imposed by the grid, it can be said that:

- the sign of the grid power reflects the flow of the grid current, which explains why the grid current and voltage are in opposition of phase (Figure 22), which means that the grid (in this mode) plays the role of a second load.
- Attenuation in the amplitude level of the grid current is explained by the small amount of power injected to the grid after fulfilling the load demand.

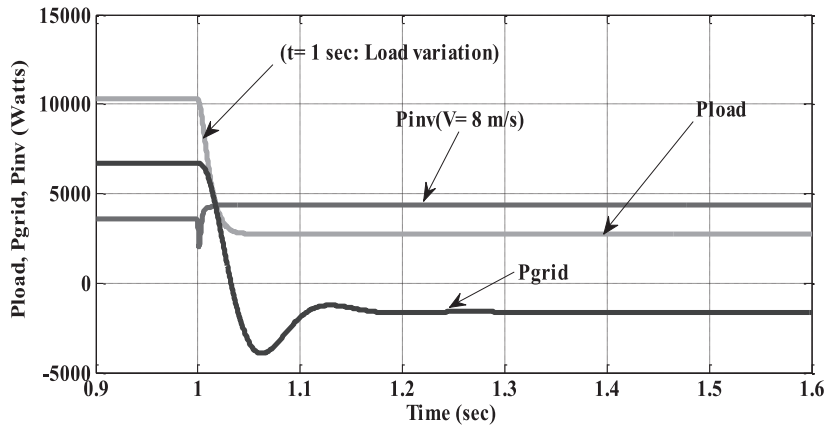


Figure 21. Active power curves after a load variation.

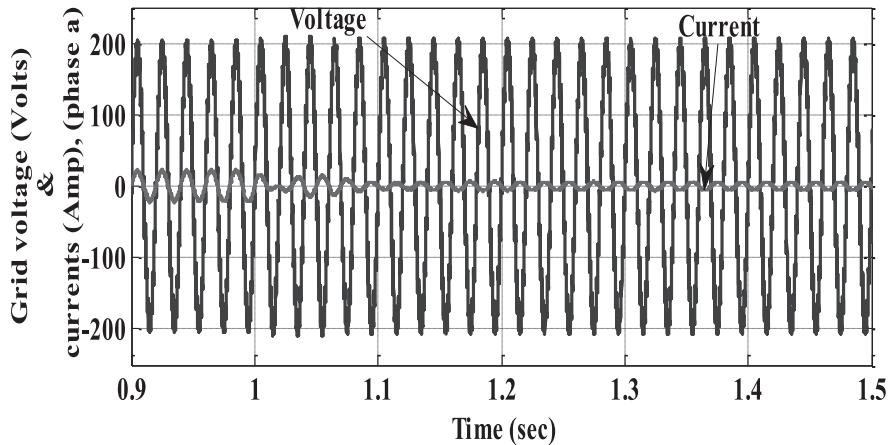


Figure 22. Grid current and voltage waveforms (phase a) after a load variation.

CONCLUSION

In the present work, we have treated the problem of harmonic pollution of power systems, its source, and adverse effects on the power grid. To remedy this problem: we improved the quality of the grid currents, reducing its THDi and increasing the power factor of the system. A modern solution based on a shunt active filter controlled by a model predictive control (MPC) and powered by a renewable energy source (wind energy generation) is introduced. The suggested MPC exploits the model of the whole system (SAPF + grid + load) to predict the behaviour of the grid currents at the next sampling time, among the eight possible voltage vectors of the SAPF; the vector that minimizes a cost function expressed as the error between the predicted and the estimated values of the grid currents will be selected and the corresponding switching state will be sent to the SAPF switches. The simplicity of the suggested MPC makes it easy to understand and implement and does not require any kind of linear controller or modulation technique.

The results confirm the feasibility of the system and validate the features assigned to the voltage source inverter, namely, the compensation of harmonic pollution, reactive power, and the transfer of the energy flow of the wind generation system part to the power grid. This novel way to interface a wind system through a two-level inverter based SAPF designed in a way to reduce the energy consumption from the utility grid by sharing the required power of a common connected load.

It is important to note that the power factor is still high, the source currents have low harmonic distortion, and the consumption of reactive power is almost zero.

APPENDIX

Table 1. Wind system parameters (Dahbi, 2012).

wParameter	Value
Nominal power (Kw)	6.6
Stator resistor R_s (Ω)	1.63
Stator inductance on the d axis L_d (H)	0.02246
Stator inductance on the q axis L_q (H)	0.02246
permanent magnet flux φ_f (Wb)	0.9
Number of pair of poles	12
Air density ρ (kg / m^3)	1.08
blade radius R (m)	3.11
Power coefficient C_{pmax}	0.5

Table 2. DC/DC converter parameters.

Parameter	Value
Inductance L (H)	0.035
Resistor R (Ω)	1 K
Capacitor C (f)	2200e-6

Submitted : 22/03/2017

Revised : 22/07/2017

Accepted : 03/12/2017

تحكم تنبؤي لمرشح فعّال للطاقة مغذى بنظام تحويل لطاقة الرياح باستعمال المولد المتزامن ذو المغناطيس الدائم

عبد القادر لخداري*، فاتح كريم*، عبد الحليم برني**

* مختبر الكترولنيات والطاقة والتحكم الصناعي، جامعة سطيف 1، الجزائر

** وحدة البحث التطبيقي في الطاقات المتجددة، مركز تنمية الطاقات المتجددة، 47133، غرداية، الجزائر

الخلاصة

يعالج هذا البحث توصيل نظام توليد طاقة الرياح بالشبكة من خلال مرشح فعّال للطاقة والذي يستخدم غالباً لتحسين نوعية الطاقة، وتعويض القدرة التفاعلية وتقليل التشوه الذي يظهر على موجات تيار الشبكة الذي تسببه الأحمال غير الخطية. مهمة أخرى مُسندة إلى المرشح الفعال، وهي حقن الطاقة النشطة المُستخرجة من نظام الرياح إلى شبكة الكهرباء وضمان تقاسم طاقة الحمل. المرشح الفعال عبارة عن عاكس ثلاثي الأطوار ذو مستويين مسيطر عليه بنظام تحكم تنبؤي ويتم تغذيته بواسطة نظام الرياح من خلال وصلة مكثف. يتم توليف متحكم تناسبى تكاملي للحفاظ على قيمة ثابتة لجهد المكثف وتعويض خسائر النظام. إن نظام طاقة الرياح مكون من توربينات الرياح موصولة بمولد متزامن ذو مغناطيس دائم بدون تروس يحول الطاقة الميكانيكية المتاحة على العمود إلى طاقة كهربائية. نتيجة للطبيعة المتقلبة غير المتوقعة للرياح وتغير سرعتها، يتم استخدام مقوم صمامات ثلاثي الأطوار موصول بمحول (DC / DC) رافع للجهد للتحكم في ونقل الطاقة الكهربائية المستخرجة من نظام الرياح إلى المكثف داخل المرشح. نتائج المحاكاة بواسطة ماتلاب سيمولينك تظهر فعالية نظام التحكم المستخدم لتحسين موجات تيار الشبكة، وتعويض القدرة التفاعلية وضمان حقن مستمر لطاقة الرياح إلى نقطة الاقتران المشترك لتقاسم طاقة الحمل مع الشبكة.